Vibronic Coupling Effects in the Photoelectron Spectrum of Ozone: A Coupled-Cluster Approach

Paweł Wójcik,[1,2] Anna I. Krylov,[1] Hannah Reisler,[1]
Péter G. Szalay,[2] and John F. Stanton[3,2,*]

[1]*Department of Chemistry, University of Southern California, Los Angeles, California 90089, USA*

[2]*Laboratory of Theoretical Chemistry,*
Institute of Chemistry, ELTE Eötvös Loránd University,
Pázmány Péter stny. 1/A, Budapest, Hungary

[3]*Quantum Theory Project, Departments of Chemistry and Physics,*
University of Florida, Gainesville, FL, USA 32611

(Dated: August 17, 2024)

One of the most important areas of application of equation-of-motion coupled cluster (EOM-CC) theory is to the prediction, simulation and analysis of various types of electronic spectra. In this work, the EOM-CC method known as EOMIP-CC is applied to the closely lying and coupled pair of states of the ozone cation – $\tilde{X}^2A_1$ and $\tilde{A}^2B_2$ – using sophisticated approaches that extend to the full singles, doubles, triples and quadruples model (EOMIP-CCSDTQ). Combined with a venerable and powerful method for calculating vibronic spectra from the Hamiltonian produced by EOMIP-CC calculations, this research provides a spectrum that is in good agreement with the photoelectron spectrum of ozone. An important result here is that the calculations suggest that the adiabatic gap separating these two electronic states is somewhat smaller than currently thought; an assignment of the simulated spectrum together with the more precise band positions of the experimental measurements suggests that this energy gap is 1366±65 cm^{-1}.

I. INTRODUCTION

Amongst the brotherhood of triatomic molecules, it cannot be argued that water (H_2O) is the most important, the most highly studied, and the most well understood. Beyond H_2O, there are many triatomic molecules that have an environmental, technological or biological

importance, have been subjected to many studied and are understood to various levels of detail. Perhaps the most interesting such case is ozone (O_3), which has a vast number of important properties, a very rich history of study[1], and – unlike the relatively simple water molecule – a profound quantum-mechanical complexity[2]. In the latter context, while we think of (and an NMR experiment would reveal) as two distinct kinds of oxygen Atoms in ozone, the full molecular Hamiltonian does not distinguish between the two types, with the three equivalent structures separated by a barrier that lies tantalizingly close to the $O_3 \rightarrow O_2 + O$ dissociation threshold (102.4 kJ/mol)[3]. In reality, the energy levels of ozone all have a near triple $(e + a)$ degeneracy, albeit with a tunneling splitting so small that it can be ignored, along with a semi-infinite lifetime (despite opposing opinion[4]). More than a half century ago, this intriguing aspect of the ozone molecule was first discussed by Berry[5].

Beyond the structural aspects of ozone, other mysteries center around this curious molecule. For example, the distribution of the eighteen distinct $^{16}O/^{17}O/^{18}O$ isotopologues in the Earth's atmosphere differs from what is expected based on the natural isotopic abundance, a puzzle that has been open for more than three decades[6].

Amongst quantum chemists, ozone has a notorious history, with its strong biradical character causing significant difficulties in calculations of its ostensibly simple ground state molecular properties. An early 1989 study[7,8] by the Bartlett group and collaborators found that the CCSD+T(CCSD) method predicted that the molecular equilibrium structure of ozone would have C_s symmetry (that is, the asymmetric stretching harmonic frequency predicted by this method was imaginary), a finding that led to a search for better treatment of non-iterative triple excitations, ultimately leading to the well-known CCSD(T) treatment[9–11]. While CCSD(T) and higher-level coupled-cluster methods available today[12–14] do a good job in predicting the molecular vibrational potential, an elaborate multireference configuration interaction study by Dawes *et al.* has done an excellent job on the entire ground-state surface out to the dissociation limit[15]. As such, the quantum chemical understanding and fidelity for the ground electronic state of O_3 is now at a mature level.

Qualitatively, the challenge posed to electronic structure by ozone ultimately arises from its closely spaced highest-occupied (b_2) and lowest-unoccupied (a_1) molecular orbitals (HOMO and LUMO, respectively). The two electron configurations $[\cdots]b_2^2a_1^0$ and $[\cdots]b_2^0a_1^2$ mix strongly, posing the aforementioned challenges with (especially single-reference) quan-

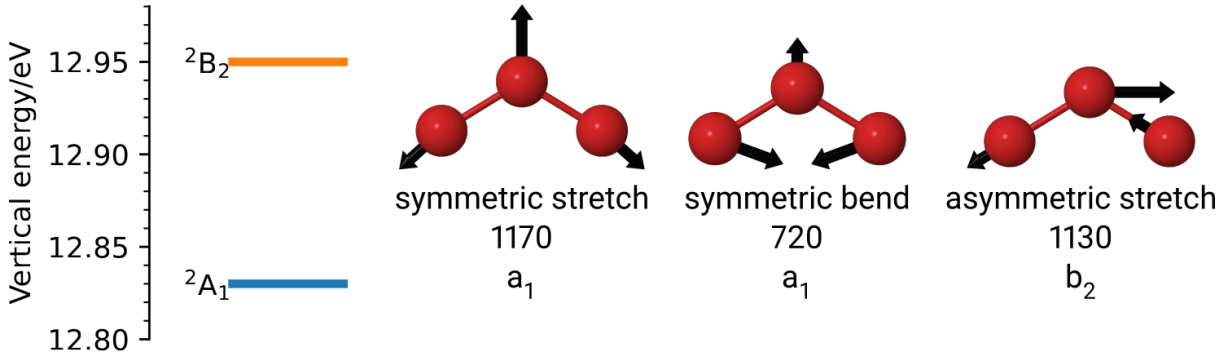

FIG. 1: Two lowest states of the ozone cation and normal modes of ozone.

tum chemical methods. Another consequence of the identity and energetic proximity of these two orbitals is that the ozone cation (which is isoelectronic to the NO_2 radical) has closely lying $^2A_1$ and $^2B_2$ electronic states. Like the associated states in NO_2, both of these states are plagued by orbital symmetry-breaking problems[16], a problem that greatly complicates quantum-chemical efforts to them. One of the many accomplishments of the Bartlett group has been the integral role played by them in the development of equation-of-motion coupled-cluster theory[17–19] (EOM-CC, also known as linear response coupled-cluster theory[20]). These methods provide a very efficient and simple way to study certain classes of what are often termed "multireference problems"[21], and are ideally suited to studying many reactive intermediates, radicals, biradicals and electronically excited states. From a somewhat wider viewpoint, the existence of closely spaced electronic states always carries the potential for (possibly strong) vibronic coupling, a phenomenon that can play an important role in molecular dynamics and spectroscopy. Indeed, one of the great successes of EOM-CC methods has been in their ability – if and only if combined with vibronic coupling models – to enable high-quality simulations of complicated electronic spectra. Such work provides important insight into the nature of vibronic coupling in molecular systems, as has been exemplified by various application studies (for example, see Refs.[22] and[23]).

Our contribution to this issue paying homage to the career and accomplishments of R.J. Bartlett consists of an application of a vibronic coupling model parametrized by EOM-CC calculations to the photoelectron spectrum of ozone. We trust that this combination of methodology applied to a molecule that has been extensively studied by the Bartlett group is an appropriate contribution to this issue.

II. THEORY

Ozone is a C_{2v} molecule (we are following the Mulliken's convention[24] by placing the molecule in the yz plane and aligning the molecular symmetry axis with the z direction) with three normal modes: symmetric stretch, symmetric bend, and asymmetric stretch. The asymmetric stretch is of a b_2 symmetry. The two lowest electronic states of the ozone cation are close in energy. The lower state is fully symmetric while the higher one is of the B_2 symmetry, the same symmetry as the asymmetric stretch. The close energetic separation and the matching symmetry of the asymmetric stretch results in significant vibronic effects appearing in the ozone photoelectron spectrum. Figure 1 presents a graphical summary of this information.

We simulate the vibronic states of the ozone cation using the model Hamiltonian of Köppel, Domcke, and Cederbaum (KDC Hamiltonian).[25–27] This is a multi-state and multi-mode Hamiltonian defined in the basis of diabatic states. We consider the ozone cation in the basis of two quasi-diabatic states coupled by one mode (mode number 3). The model also includes two symmetric modes (modes number 1 and 2)

$$H = H_0 \mathbf{1} + \begin{pmatrix} V^{(1)} & \lambda_3 Q_3 \\ \lambda_3 Q_3 & V^{(2)} \end{pmatrix} \tag{1a}$$

$$H_0 = \frac{1}{2}\left(\sum_{i=1}^{3} -\omega_i \frac{\partial^2}{\partial Q_i^2}\right) + \frac{1}{2}\omega_3 Q_3^2 \tag{1b}$$

$$V^{(\alpha)} = E^{(\alpha)} + \sum_{i,j,k,l\in\{1,2\}} \kappa_i^{(\alpha)} Q_i + \kappa_{ij}^{(\alpha)} Q_i Q_j + \kappa_{ijk}^{(\alpha)} Q_i Q_j Q_k + \kappa_{ijkl}^{(\alpha)} Q_i Q_j Q_k Q_l. \tag{1c}$$

The Hamiltonian parameters are expanded around the equilibrium geometry of ozone. $E^{(\alpha)}$ are the vertical ionization energies calculated at that geometry. Q_i are the dimensionless normal coordinates of ozone. κ are the coefficients of expansion of the potential along the fully symmetric coordinates. λ are the linear diabatic couplings. ω are the harmonic frequencies of ozone.

We find the parameters that enter the KDC Hamiltonian using *ab inito* coupled-cluster (CC) methods and its equation-of-motion EOM-CC extension.[19,21,28–31] We use the CC truncated to singles and doubles (CCSD), singles, doubles and triples (CCSDT) as well as singles, doubles, triples and quadruples (CCSDTQ).[14] We use the EOM-CC for ionization potential (EOM-IP).[32] We use the Ichino, Gauss and Stanton definition of quasi-diabatic states based

on the EOM-CC method (EOM-CC-QD)[33]. In all CC and EOM-CC calculations we leave all electrons correlated, in other words, we do not use the frozen-core approximation.

Using CCSDT/ANO1 we optimize the geometry of ozone and compute its harmonic frequencies and normal coordinates.[34,35] At the same geometry we compute the linear diabatic coupling λ using EOM-IP-CCSD-QD/ANO1. We use EOM-IP-CCSDT/ANO1 on a grid to find the expansion coefficients κ.

The vertical ionization energies are calculated using a composite method. The base value is the complete basis set (CBS) extrapolation of the EOM-IP-CCSDT/cc-pCVnZ energies with n = 5, 6.[36] These values are augmented with two corrections: the ΔQ correction in the cc-pwCVTZ basis set and the relativistic correction calculated using EOM-IP-CCSD/cc-pwCVTZ.[37] We introduce an error estimates to the reported vertical energies. For the error estimate of the extrapolated CBS value we use half of the absolute value of the difference between the best *ab initio* value and the extrapolated value. For the remaining corrections we use as the error estimate half of the absolute value of the correction.

To compare the simulated photoelectron spectrum to the experimental one, we use the oscillator strengths ratio A_1:B_2 of 1:1.35.[38] Additionally, the stick spectrum is broadened with the Lorenzian envelopes normalized to the peaks' intensities

$$f_{envelope}(x, x_i, I_i) = \frac{I_i}{(x - x_i)^2 + (\gamma/2)^2}. \tag{2}$$

x_i is the position of the spectral peak, I_i is its intensity and γ is the peak's width.

We use the XSIM program of Dr. Stanton to simulate the spectrum using the basis of 50 harmonic states in each mode and 6000 iterations of the Lanczos procedure. All remaining *ab initio* calculations are completed using CFOUR.[39,40]

III. RESULTS

The optimized geometry of ozone gives the bond lengths of 1.270 Å and the bond angle of 116.9°. The two symmetric normal modes have frequencies 1169 cm^{-1} and 724 cm^{-1}, while the asymmetric stretch has frequency equal to 1129 cm^{-1}. The computed value of the linear diabatic coupling constant λ is 1394 cm^{-1}. The vertical ionization energy for the first excited state, $E^{(1)}$, computed using the composite method described above is equal to 12.827 eV. Our error estimate for this value is 30 meV, see Table I for details. We note that

TABLE I: Vertical ionization energies with the error estimates, eV.

Contribution	$^2A_1$	$^2B_2$	Error estimate
CBS	12.872	12.981	0.02
ΔQ	-0.037	-0.021	0.02
Relativistic	-0.008	-0.010	0.005
Sum	12.827	12.950	0.03

TABLE II: The energy gap between vertical ionization energies of the $^2A_1$ and $^2B_2$ states with error estimates, meV. See caption of Table I.

Contribution	Gap	Error estimate
EOM-CCSDT/CBS	108.8	0.9
ΔQ/pwCVTZ	16.5	8
Relativistic/CCSD/pwCVTZ	-2.2	1.1
Final value, meV	123	8
Final value, cm^{-1}	990	65

the convergence of the vertical ionization gap between the two states is much faster and we estimate this value as equal to 123 ± 8 meV, see Table II for details.

Figure 2 compares the simulated spectrum to the experimental one taken from reference[41]. Our simulation allows for an additional element of analysis of the simulated spectrum. Figure 3 presents a decomposition of the simulated spectrum from Figure 2. All lines that contribute to the spectrum are marked individually and are color-coded indicating which electronic state's transition intensity the peak draws from. The total envelope of the spectrum is also decomposed showing contributions from both states. Our simulation locates the minimum of the conical intersection at 3174 cm^{-1} above the origin (12.92 eV) that is marked on the figure as CI.

We would like to assign the vibronic peaks from our simulation. To this end, we run the simulation once again, this time, however we set the linear diabatic constant to zero, i.e., $\lambda = 0$. With that change we can reproduce the spectrum (at an equivalent level of theory)

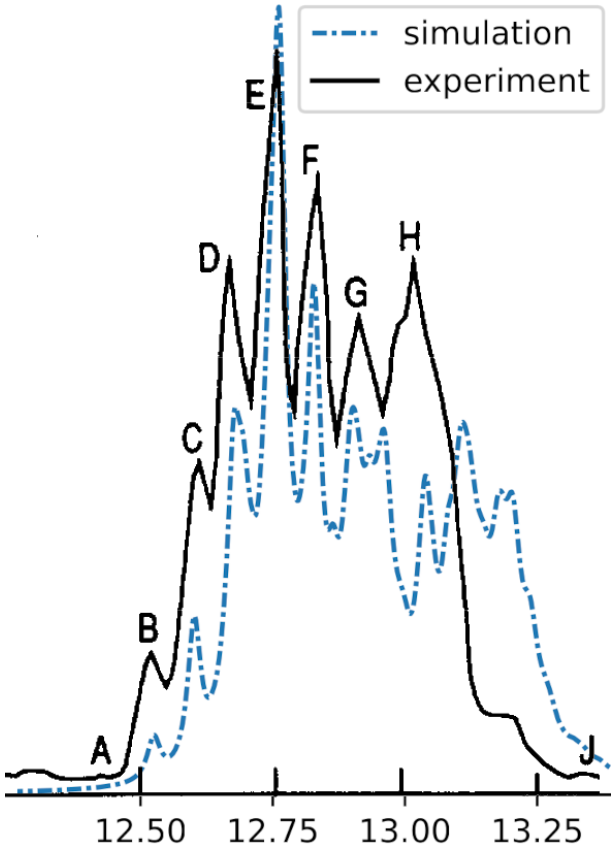

FIG. 2: Comparison of the experimental (solid black line) and the simulated spectrum. In the simulated spectra the plot is generated with peak width $\gamma = 30$ meV. The simulated spectrum is shifted towards higher energies by 21 meV.

but in an artificial case where there is no vibronic coupling. Figure 4 presents this spectrum. The non-coupled spectrum is easy to assign using the labels that mark the symmetry of the electronic state, A_1 or B_2, and the vibrational state $(\nu_1\nu_2\nu_3)$, where ν_i is the number of quanta in mode i with $i = 1$ for the symmetric stretch, $i = 2$ for the symmetric bend and $i = 3$ for the asymmetric stretch. The assigned spectrum shows progressions in the symmetric bend. There is one such progression in each electronic state. Additionally for each state, there is also another progression in the symmetric bend with one excitation in the symmetric stretch.

We decompose the vibronic states of our main simulation in the basis of the artificial, uncoupled states discussed in the previous paragraph. Figure 5 shows the assigned spectrum and Table III lists the decomposition of all peaks in the region of up to 3000 cm^{-1} with intensities larger than 10^{-3}. We compare the assigned spectrum against the high-

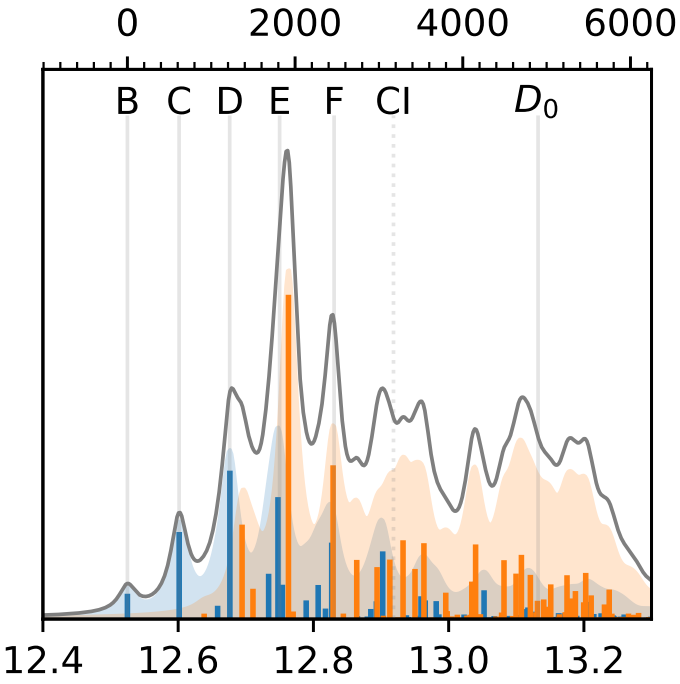

FIG. 3: Simulated photoelectron spectrum of ozone. Bottom axis shows energy scale in eV. Top axis shows energy offset from the origin in cm^{-1}. Stick spectrum shows positions and intensities of all simulated states. Blue color corresponds to the oscillator strength originating from the $^2A_1$ basis state while the red one corresponds to $^2B_2$. Gray vertical lines with captions on top indicate positions of features as measured by the PFI-ZEKE experiment.[42] The simulated spectrum was shifted to match the PFI-ZEKE experimental origin. D_0 marks the dissociation threshold of O_3^+. Gray dotted line marks the energy of the minimum of the conical intersection (CI).

resolution pulsed-field-ionization zero-kinetic-energy (PFI-ZEKE) spectrum from 2005.[42] The PFI-ZEKE spectrum is the best source of information on the location of the peaks, especially the origin, against which align our simulation. The origin of the simulated spectrum is located 170 cm^{-1} lower than the experimental origin which was experimentally observed at $101,020.5$ cm^{-1}.[42] This is within our error estimate for the vertical ionization energy (30 meV= 240 cm^{-1}).

Lastly, we compare our simulation to an earlier accurate simulation, the work of Tarroni and Carter from 2011.[43] Figure 6 presents a comparison of lines from both simulations. The comparison includes only the lines from the earlier simulation that were tabulated with an

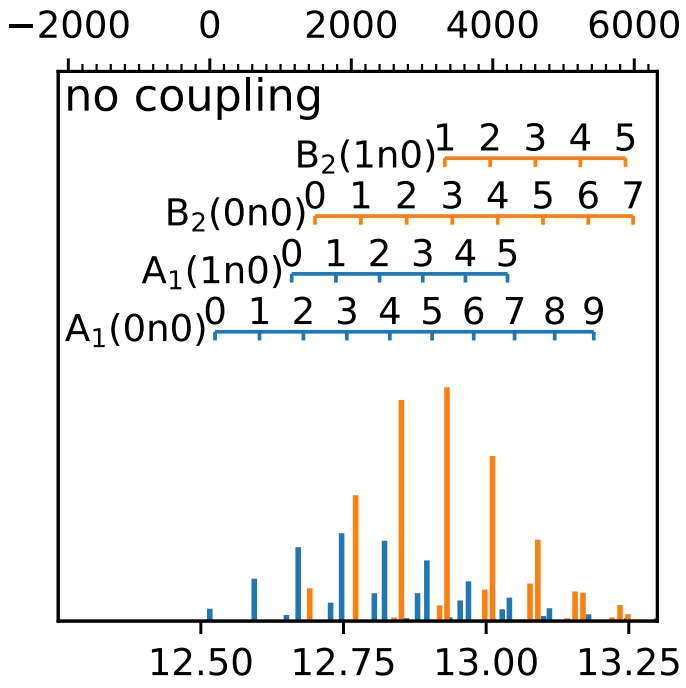

FIG. 4: Simulated photoelectron spectrum of ozone, but with no account given to the vibronic coupling effect.

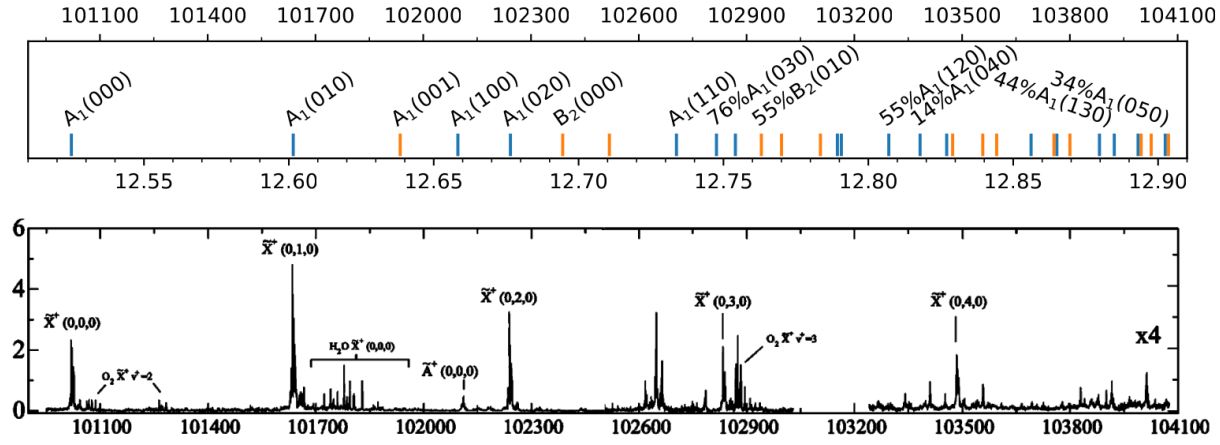

FIG. 5: Comparison of the simulated spectrum with the PFI-ZEKE experiment.[42] The simulated spectrum was shifted by 21 meV= 170 cm^{-1} towards higher energies.

assignment.

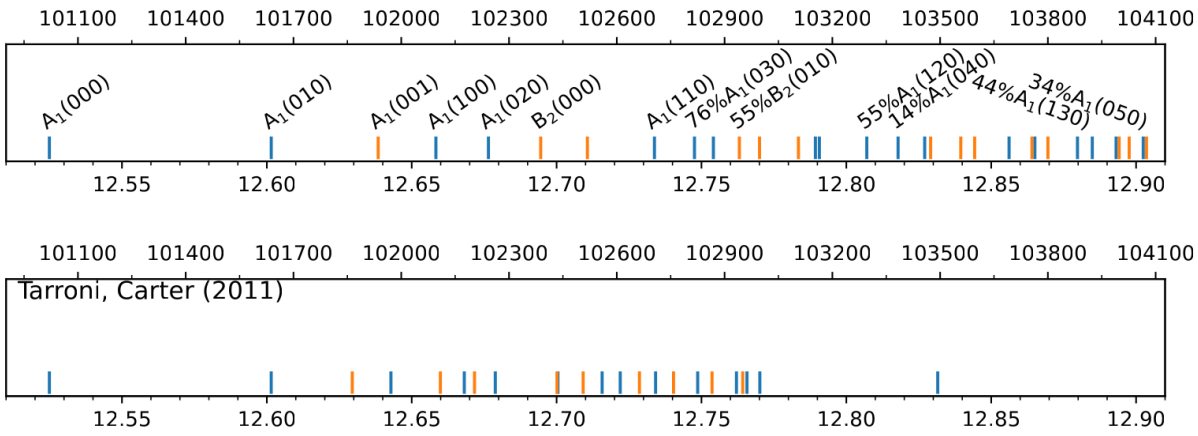

FIG. 6: Comparison of the simulated spectrum to an earlier accurate simulation of Tarroni and Carter (assigned lines).[43]

IV. DISCUSSION

We first discuss the comparison of our simulations to the lower-resolution experimental spectrum presented on Figure 2. The peak A is known to be a hot band.[38] The simulation reproduces well the consecutive increase in the intensities of peaks B, C, D, and E. The spacing between these peaks is also well reproduced. Drop in the intensity at the peak F is captured by the simulation. Starting from the peak G, the simulation shows discrepancy with the experiment. A sudden drop in the intensity past the peak H is not observed in the simulation. We discuss a likely source of this mismatch later.

The decomposition of the spectrum presented on Figure 3 introduces additional insight. The spectrum shows that peaks B and C are almost purely of the $^2A_1$ character. Starting from the peak D, the contributions from two states are equally important. It is also clear that the following peaks arise as mixtures of many vibronic peaks. At the energy of about 2000 cm^{-1} above the origin the density of vibronic peaks increases significantly. This value can be compared to the minimum of the conical intersection located about 1000 cm^{-1} higher. Our simulation is incapable of accounting for dissociation of the molecule, therefore we expect a discrepancy with the experiment as the energy gets closer to the dissociation threshold located at 4840 cm^{-1} above the origin.[42]

Moving on to the comparison with the high-resolution spectrum, see Figure 5, reveals more details. Lines of the PFI-ZEKE experiment and our simulation show a good match. Especially the states with an oscillator strength originating from the A_1 state are well aligned

TABLE III: Assignment and decomposition of the eigenvectors of the ozone cation.

Peak position (cm^{-1})	Assignment	Eigenvector
0	$A_1(000)$	$-0.99\ A_1(000)$
618	$A_1(010)$	$+0.99\ A_1(010)$
915	$A_1(001)$	
1076	$A_1(100)$	$-0.99\ A_1(100)$
1222	$A_1(020)$	$-0.97\ A_1(020)$
1368	$B_2(000)$	$+0.97\ B_2(000)$
1498		$-0.10\ B_2(000)$
1684	$A_1(110)$	$-0.96\ A_1(110)$
1796	$A_1(030)$	$-0.87\ A_1(030) - 0.16\ A_1(110) - 0.13\ A_1(020) + 0.13\ A_1(040)$
1848		$+0.31\ A_1(030)$
1921	$B_2(010)$	$-0.74\ B_2(010) + 0.18\ B_2(020) + 0.11\ B_2(000)$
1977		$+0.24\ B_2(010)$
2085		$-0.52\ B_2(010)$
2132		$+0.25\ A_1(030) + 0.24\ A_1(040) + 0.13\ A_1(120) - 0.13\ A_1(050)$
2275	$A_1(120)$	$+0.86\ A_1(120) + 0.12\ A_1(040)$
2363		$-0.62\ A_1(040) + 0.40\ A_1(120) - 0.17\ A_1(030) + 0.11\ A_1(050)$
2439		$+0.47\ A_1(040) + 0.12\ A_1(120)$
2454		$+0.53\ B_2(020) + 0.24\ B_2(010) - 0.17\ B_2(030)$
2576		$+0.27\ B_2(020)$
2736		$+0.60\ B_2(020)$
2886	$A_1(130)$	$-0.81\ A_1(130) + 0.12\ A_1(050) - 0.10\ A_1(120)$
2974		$-0.24\ B_2(110) - 0.16\ B_2(020)$
3047	$A_1(050)$	$+0.76\ A_1(050) + 0.13\ A_1(130)$

with the experimental features. States close to the origin are similar to the non-coupled states. The origin peak is of a clear $A_1(0,0,0)$ character, the first two excitations in the symmetric bend, $A_1(0,1,0)$ and $A_1(0,2,0)$ are also very similar to the non-coupled states, while the higher excitations in this progression are showing large mixing. The same progression with one vibrational quantum in the symmetric stretch is more interesting. The first of its peaks is very well aligned with an experimentally visible feature, which was previously assigned as the origin of the second state. The second peak in this series, the first combination state $A_1(1,1,0)$, has very high similarity to its uncoupled version. It is a good candidate to assign the experimental, unassigned feature above $102,600\ cm^{-1}$.

States with an oscillator strength from the B_2 state are, on the other hand, not aligning

well with the experiment. First such peak, close to the 12.64 eV mark on Figure 5, is of a vibronic character and we assign it as a $A_1(0,0,1)$ state which gains intensity thanks to the coupling to the B_2 state. This vibronic peak lies in the part of the spectrum marked as pollution due to water. The origin of the B_2 state is very similar to the uncoupled $B_2(0,0,0)$ state, but it is located in an empty area of the experimental spectrum. The next peak, slightly above the 12.76 eV mark on Figure 5, corresponds to the one excitation of the symmetric bend in the B_2 state, but as the label on the figure shows, it is only about 55% similar to the uncoupled state.

The comparison to the earlier simulation on Figure 6 shows that both present a good match to the experiment. Both simulations also agree in the assignment of the first progression in the bending mode. The previous simulation, however, shows smaller spacing between the remaining lines, showing much higher congestion of the spectrum. Additionally the origin of the second state falls at lower energy aligning well with the peak that was assigned in the PFI-ZEKE experiment also as the origin of the second state. While an additional simulation of the line intensities would allow for the most complete comparison to the experimental spectrum, the strong alignment of the simulated peaks of a leading A_1 character with the experimental features leads us to believe that our simulation offers the best assignment of the spectrum to date.

V. SUMMARY AND CONCLUSIONS

We have simulated the vibronic effects in the photoelectron spectrum of the ozone. We have used the KDC Hamiltonian[25–27] with the *ab initio* parametrisation of the quasi-diabatic states of Ichino, Gauss and Stanton.[33] The results of our simulation match well the photoelectron spectrum from 1970s[41] and the PFI-ZEKE spectrum from 2005.[42] We present analysis of the spectra and highlight the role of the vibronic coupling effects. Our simulation offers a state-of-the-art insight into the spectrum and allows us to assign the simulated peaks. Our assignment agrees well with the previously assigned progression in the symmetric bend but we reassign some of the other features of the spectrum. Simulated peaks that gain intensity from the B_2 state are absent in the PFI-ZEKE spectrum which offers an interesting avenue for further investigations. Modeling of the intensity of the PFI-ZEKE peaks is not unlikely to bring insight into this problem. Additionally our simulation does not model dissociation

of the ozone cation, which will play a role in the high energy part of the spectrum.

VI. ACKNOWLEDGMENTS

This project was initiated when three of the authors (P.W, P.G.S. and J.F.S) were in Budapest, where J.F.S. was serving as a recipient of the John von Neumann Award in STEM bestowed by the Fulbright Foundation. Additional research presented here benefited from the NSF Center for Chemical Innovation Phase I (grant no. CHE-2221453) and the U.S. Department of Energy, Basic Energy Sciences (grant no. DE-FG02-05ER15629). All the authors of this research wish Prof. Bartlett a happy ninth decade of life, and hope that he continues to stimulate others in the field with his creative insights.

* Electronic address: jfstanton137@gmail.com

[1] J. Chappuis, Ann. d. l'ecole Norm. Sup. **11**, 159 (1882).

[2] D. Babikov, B. K. Kendrick, R. B. Walker, R. Schinke, and R. T. Pack, Chem. Phys. Lett. **372**, 686 (2003).

[3] B. Ruscic and D. H. Bross, *Active Thermochemical Tables (ATcT) Thermochemical Values ver. 1.130* (2023), URL https://www.osti.gov/biblio/1997229.

[4] P. Garcia-Fernandez, I. B. Bersuker, and J. E. Boggs, Phys. Rev. Lett. **96**, 163005 (2006).

[5] R. S. Berry, Rev. Mod. Phys. **32**, 447 (1960).

[6] B. Schueler, J. Morton, and K. Mauersberger, Geophys. Res. Lett. **17**, 1295 (1990).

[7] J. F. Stanton, W. N. Lipscomb, D. H. Magers, and R. J. Bartlett, J. Chem. Phys. **90**, 1077 (1989).

[8] D. H. Magers, W. N. Lipscomb, R. J. Bartlett, and J. F. Stanton, J. Chem. Phys. **91**, 1945 (1989).

[9] K. Raghavachari, G. . Trucks, J. A. Pople, and M. Head-Gordon, Chem. Phys. Lett. **157**, 479 (1989).

[10] M. Urban, J. Noga, S. J. Cole, and R. J. Bartlett, J. Chem. Phys. **83**, 4041 (1985).

[11] J. D. Watts, J. Gauss, and R. J. Bartlett, J. Chem. Phys. **98**, 8718 (1993).

[12] S. A. Kucharski and R. J. Bartlett, J. Chem. Phys. **97**, 4282 (1992).

[13] M. Kállay and P. R. Surján, J. Chem. Phys. **115**, 2945 (2001).

[14] D. A. Matthews and J. F. Stanton, J. Chem. Phys. **142** (2015).

[15] R. Dawes, P. Lolur, A. Li, B. Jiang, and H. Guo, J. Chem. Phys. **139** (2013).

[16] C. F. Jackels and E. R. Davidson, J. Chem. Phys. **64**, 2908 (1976).

[17] J. F. Stanton and R. J. Bartlett, J. Chem. Phys. **98**, 7029 (1993).

[18] M. Nooijen and R. J. Bartlett, J. Chem. Phys. **102**, 3629 (1995).

[19] R. Bartlett and M. Musiał, Rev. Mod. Phys. **79**, 291 (2007).

[20] H. Koch and P. Jørgensen, J. Chem. Phys. **93**, 3333 (1990).

[21] A. I. Krylov, Annu. Rev. Phys. Chem. **59**, 433 (2008).

[22] J. F. Stanton, J. Chem. Phys. **126**, 134309 (2007).

[23] H. Köppel, M. Döscher, I. Baldea, H.-D. Meyer, and P. G. Szalay, J. Chem. Phys. **117**, 2657

(2002).

[24] R. S. Mulliken, J. Chem. Phys. **23**, 1997 (1955).

[25] H. Köppel, W. Domcke, and L. Cederbaum, Adv. Chem. Phys. **57**, 59 (1984).

[26] W. Domcke, H. Köppel, and L. S. Cederbaum, Mol. Phys. **43**, 851 (1981).

[27] H. Köppel, W. Domcke, and L. S. Cederbaum, *The multi-mode vibronic-coupling approach* (World Scientific Publ Co Pte Ltd, 2004), chap. 7, pp. 323–367.

[28] I. Shavitt and R. J. Bartlett, in *Many-body methods in chemistry and physics: MBPT and coupled-cluster theory* (Cambridge University Press, Cambridge, 2009).

[29] K. Sneskov and O. Christiansen, WIREs: Comput. Mol. Sci. **2**, 566 (2012).

[30] R. J. Bartlett, WIREs: Comput. Mol. Sci. **2**, 126 (2012).

[31] A. I. Krylov, in *Reviews in Comp. Chem.*, edited by A. L. Parrill and K. B. Lipkowitz (J. Wiley & Sons, 2017), vol. 30, pp. 151–224.

[32] J. F. Stanton and J. Gauss, J. Chem. Phys. **111**, 8785 (1999).

[33] T. Ichino, J. Gauss, and J. F. Stanton, J. Chem. Phys. **130**, 174105 (2009).

[34] J. Almlöf and P. Taylor, J. Chem. Phys. **86**, 4070 (1987).

[35] J. Almlof, T. Helgaker, and P. R. Taylor, J. Phys. Chem. **92**, 3029 (1988).

[36] D. Woon and T.H. Dunning, Jr., J. Chem. Phys. **103**, 4572 (1995).

[37] K. A. Peterson and T. H. Dunning, Jr., J. Chem. Phys. **117**, 10548 (2002).

[38] H. Müller, H. Köppel, L. S. Cederbaum, T. Schmelz, G. Chambaud, and P. Rosmus, Chem. Phys. Lett. **197**, 599 (1992).

[39] J. Stanton, J. Gauss, M. Harding, and P. Szalay, *CFOUR*, with contributions from A.A. Auer, R.J. Bartlett, U. Benedikt, C. Berger, D.E. Bernholdt, Y.J. Bomble, L. Cheng, O. Christiansen, M. Heckert, O. Heun, C. Huber, T.-C. Jagau, D. Jonsson, J. Jusélius, K. Klein, W.J. Lauderdale, F. Lipparini, D.A. Matthews, T. Metzroth, L.A. Mück, D.P. O'Neill, D.R. Price, E. Prochnow, C. Puzzarini, K. Ruud, F. Schiffmann, W. Schwalbach, C. Simmons, S. Stopkowicz, A. Tajti, J. Vázquez, F. Wang, J.D. Watts; and the integral packages MOLECULE (J. Almlöf and P.R. Taylor), PROPS (P.R. Taylor), ABACUS (T. Helgaker, H.J.Aa. Jensen, P. Jørgensen, and J. Olsen), and ECP routines by A.V. Mitin and C. van Wüllen. For the current version, see http://www.cfour.de.

[40] D. A. Matthews, L. Cheng, M. E. Harding, F. Lipparini, S. Stopkowicz, T.-C. Jagau, P. G. Szalay, J. Gauss, and J. F. Stanton, J. Chem. Phys. **152**, 214108 (2020).

[41] J. M. Dyke, L. Golob, N. Jonathan, A. Morris, and M. Okuda, J. Chem. Soc., Faraday Trans. 2 **70**, 1828 (1974).

[42] S. Willitsch, F. Innocenti, J. M. Dyke, and F. Merkt, J. Chem. Phys. **122** (2005).

[43] R. Tarroni and S. Carter, Chem. Phys. Lett. **511**, 201 (2011).